FIRST EXPERIMENTAL EVIDENCE OF WIND AND SWELL SIGNATURES IN L5 GPS AND E5A GALILEO GNSS-R WAVEFORMS

J.F. Munoz-Martin[1], R. Onrubia , D. Pascual , H. Park[1], A. Camps[1],
C. Rüdiger[2], J. Walker[2], and A. Monerris[3]

[1]CommSensLab - UPC, Universitat Politècnica de Catalunya – BarcelonaTech, and IEEC/CTE-UPC
[2]Department of Civil Engineering, Monash University, Clayton, VIC 3800, Australia
[3]Department of Infrastructure Engineering, The University of Melbourne, Parkville, VIC 3010, Australia,
e-mail: joan.francesc@tsc.upc.edu, camps@tsc.upc.edu

ABSTRACT

As compared to the using L1C/A signals, L5/E5a Global Navigation Satellite System - Reflectometry (GNSS-R), gives improved resolution over the Earth's surface due to the sharper auto-correlation function. Furthermore, the larger transmitted power (+3dB with respect to L1 C/A), and correlation gain (+40dB) allows the reception of weaker reflected signals. If high directivity antennas are used, very short incoherent integration times are needed to have enough signal-to-noise (SNR) ratios, allowing the reception of multiple specular reflection points such as crest of consecutive waves without the blurring induced by long incoherent integration times. This study presents for the first time experimental evidence of the wind and swell waves signatures in the GNSS-R waveforms, and compares them with models.

Index Terms— GNSS-R, Waveform, GPS, Galileo, Sea, Swell, Waves

1. INTRODUCTION

The Microwave Interferometric Reflectometer (MIR) [1, 2] is an airborne GNSS-R (Fig. 1) instrument conceived to perform cGNSS-R and iGNSS-R using dual-band (L1/E1 and L5/E5a), high directive up-looking and down-looking antenna arrays. The MIR instrument was conceived for real-time processing, but the raw data was also stored at 1-bit with 32 MS/s in a massive storage device for offline processing. One of the MIR maiden flights was over the Bass Strait that sep- arates Australia and Tasmania. The large directivity of the MIR antennas allows a clear detection of the reflected signalwith short incoherent integration times (40-300 ms). In these conditions, the peak of the reflected signal is not blurred, and re-tracking is not required. In addition, the high directivity of the antennas allowed to study secondary specular reflections in the same Delay-Doppler Map (DDM) or waveform (WF) provided they occur within the 3dB antenna beam-width. In this study, we present the impact of this Bragg forward scattering in the WFs, and how this information can be used to infer parameters of the sea state.

(a) (b)

Fig. 1: (a) Microwave interferometric reflectometer (MIR) instrument and up-looking array mounted inside the airplane, and (b) down-looking array covered with a radome hanging from the airplane's fuselage [1]

2. MIR DATA DESCRIPTION

The data under analysis correspond to a flight over the Bass Strait on June 6th, 2018. The plane was flying at a height of 1500 meters at a mean speed of 74 m/s. The data used correspond to three passes following a line that goes from 38.67º S, 149,13º E to 38.88º S, 149.11º E, as detailed in Fig. 2. Data used was sampled at 32 MS/s, packetized, and time-tagged once every 300 ms. In order to ease the data processing scheme, a single 300 ms packet is used for a single waveform, but a much shorter integration time of 40 ms was selected to avoid blurring of the waveform due to the plane movement. For the plane speed (74 m/s), the incoherent integration time (40 ms), the blurring corresponds to an integration over 3m. of sea. In addition, the generation rate of the waveform (i.e. the final observable) is 300 ms, thus each measurement is separated 22 meters.

MIR is able to track two L1 and two L5 beams at the same time, during the track shown in Fig. 2. Table 1 summarizes the incidence angle of the GNSS signals depending on the beam and the number of pass. In this study only the L5 beams

are processed due to narrower auto-correlation function, and higher SNR.

Table 1: Track and beam PRN and mean incidence angle of the measurement

Track ID	Beam ID	Constellation and PRN	Incidence angle (º)
1	1	GPS #1	39-40
1	2	GPS #32	51-52
2	1	GPS #1	36-37
2	2	GALILEO #8	49-50
3	1	GALILEO #8	35-36
3	2	GPS #3	35-37

(a) (b) (c)

Fig. 2: Position of the plane superposed to (a) wind-driven wave period, (b) swell wave period, and (c) wind speed over sea of the data used for the secondary specular reflection analysis

The processing of the L5 beams, showed that most of the L5 waveforms contained a second specular peak some delays bins apart from the specular one. In order to understand its origin, the sea state conditions during the flight were studied. As there is a lack of in situ buoy information in the area, the history from the ICON model [3] was downloaded [4], the maps downloaded are shown in Fig. 2 as (a) wind wave period [s], (b) swell wave period [s], and (c) wind speed over the sea [m/s]. The waves shown in Fig. 2 (a) have a period of τ_{wind} 5 seconds, and they are moving with an look an- gle with respect to the plane trajectory of 50º. The swell waves (2 (b)) have a period of τ_{swell} 9 seconds, and the look angle with respect to the plane trajectory is 120º. The wave-driven waves period is related with the wave speed and therefore the wavelength [5] (i.e. distance between the crests of the wave), as in (1).

$$C_{waves} = 1.56 \cdot T_{waves}$$
$$\Lambda_{waves} = C_{waves} \cdot T_{waves} \quad (1)$$

where C_{waves} is the sea celerity (or speed [m/s]), and T_{waves} is the wave period (in [s]). In deep water conditions, the relationship between them is the above closed formula.

In the case under study, the wavelengths of the mixture between wind waves and swell waves is between 39 meters and 126 meters. However, as stated in [6], most ocean waves are a combination of waves, thus producing lower periods between waves (i.e. shorter wavelengths).

3. SEA WAVELENGTH RETRIEVAL FROM WAVEFORMS

The reflection scenario (detailed in Fig. 3) is not flat, and due to the roughness produced by the combination of both swell waves and wave-driven waves, multiple reflections are produced and captured by the antenna footprint. The first Fresnel zone (i.e. the area that contains the specular reflection) in the described scenario has a length of $l_{Fz} = \sqrt{\lambda \cdot h} = 18.5$ m. Thus, nearby areas such as successive wave crests out of the first Fresnel zone may produce different reflections that are added constructively or destructively in the receiver antenna.

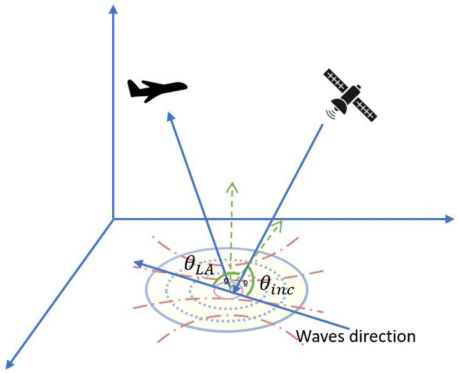

Fig. 3: Reflection scenario, defining ϑ_{LA}, the look angle of the waves, and ϑ_{inc}, the incidence angle

When the GNSS signal wavefront arrives to a sea wave series it is then Bragg forward scattered produced an interference pattern depending on the region where the signal has been reflected. As an example, a wavefront perfectly reflected over two wave crests as in Fig. 4 produces a constructive addition in the receiver antenna, hence it is detected as a second or even a third peak in the processed waveform. Note that, due to the geometry, the vector formed between the plane-to-specular, and its angle with respect to the waves direction of propagation, different peak-to-peak distances may appear in consecutive waveforms.

In order to retrieve this second peak position the waveform is re-sampled using a Fourier interpolation (i.e. by inverse FFT of the zero-padded FFT of the waveform), and then finding the local maxima of the interpolated waveform. The first two maxima of the waveform are computed to retrieve the distance between two consecutive wave crests. The difference in samples between the two peaks position is then converted into meters 2.

$$\Delta_m = \Delta_{samples} \cdot \frac{c}{K \cdot f_s} \quad (2)$$

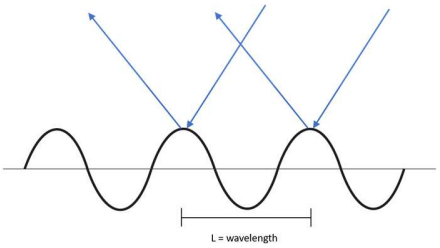

Fig. 4: Bragg forward scattering over two wave crests

where c is the light speed, f_s is the instrument sampling frequency, and K the re-sampling ratio applied prior to the find peak function.

4. RESULTS

The algorithm has been implemented with $K = 8$ and applied to several waveforms for both GPS L5 and Galileo E5a signals. The resulted waveforms used in this analysis present different multiple peaks and also different shapes of the specular peak. In this study, different waveforms are analyzed in order to understand the presence of a second and third peak in the reflected signal and its relation to the distance between crest of waves. This section contains a detailed analysis of different consecutive waveforms (i.e. separated 300 ms one from each other) at different incidence angles and different constellations (GPS and Galileo).

Figure 5 shows four examples of time consecutive waveforms reflected on the sea surface. As seen in 5a, three peaks are identified in the waveforms, 21 and 68 lags apart from the first peak, which converted in meters using (2) correspond to 24 m. and 79 m. In this case, the amplitude of the second and third peak is comparable to the specular one. The next example (5b) shows that the second peak has been shifted 3 samples, and the third peak has decreased in amplitude and also has advanced 4 samples, which it turns the peak-to-peak distance measure to 28 m. and 74 m. respectively. The third consecutive waveform shows both peaks have signifi- cantly moved, and now the distance between peaks is 55 m. and 83 m. respectively. Finally, the last waveform shows that the secondary reflection has almost dissipated, but a non-constructive multi-path due to multiple reflections over the sea is shown as a blurring of the L5 tail.

The next waveform set corresponds to the same time moment as Fig. 5, but from the second GPS L5 beam from MIR. The difference of both measurements is the incidence angle and the specular reflection position. Figure 6 contains less peaky waveforms, with two of them (6a and 6c) with the same phenomena as Fig. 5d. However, both 6b and 6c (which are not consecutive but separated 600 ms one from each other) contain the second peak very close one to each other, 6b with 45 m. of distance and 6d with 51 m. of distance between

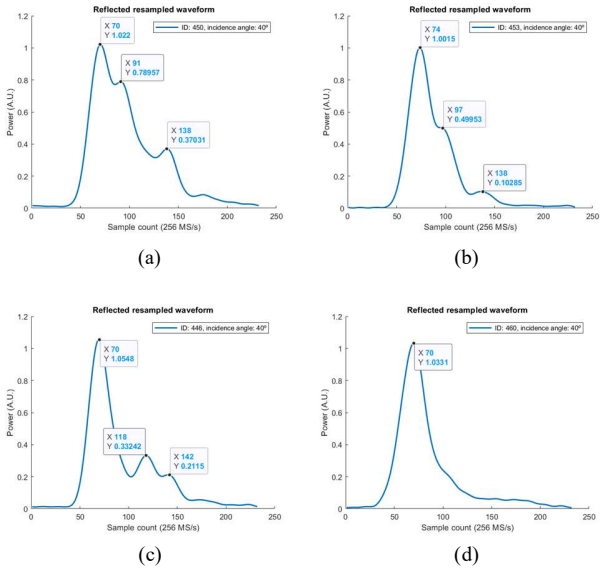

Fig. 5: GPS L5 reflected waveforms over the sea (beam 1) with multiple peaks present in the reflected waveform for cases (a), (b), and (c), and a blurry of the tail of the reflected waveform for case (d)

peaks. Waveform 6b suffers from a widening of the main peak, which may indicate that the specular reflection point has been also contaminated by a very close reflection in the glistening zone a couple of delays away (i.e. as in Fig. 5a but even closer, which causes this widening).

The last example corresponds to a set of Galileo E5a waveforms (Fig. 7). Note that, in this case the plane position and time is not the same as in figures 5 and 6. In this last set of waveforms it is identified a main secondary peak that is moving around the specular reflection, waveforms 7a and 7c have both a peak separation of 57 m. and 56 m. respectively, while 7b and 7d have 43 m. and 35 m. of peak separation. Moreover, 7c has the same widening effect than the one identified in Fig. 6b. Looking at this set of waveforms, it is identified that the radiation pattern produced by the Bragg forward scattering on the different waves depending on the look angle is modulating both the amplitude and the peak-to-peak distance. Finally, a third peak is identified also in the fourth Galileo E5a waveform (7d) which has a distance to the first peak of 72 m.

Taking into consideration the wind-driven and swell wave characteristics explained in section 2, the distances inferred from the peak-to-peak position in previous figures is inside the range provided by the ICON model, between 39 m. and 126 m. As shown in [6], analyzing the peak-to-peak distance with different methods (i.e. statistical, time, and frequency domain analysis) the swell and wind-driven period can be estimated using L5 GNSS waveforms.

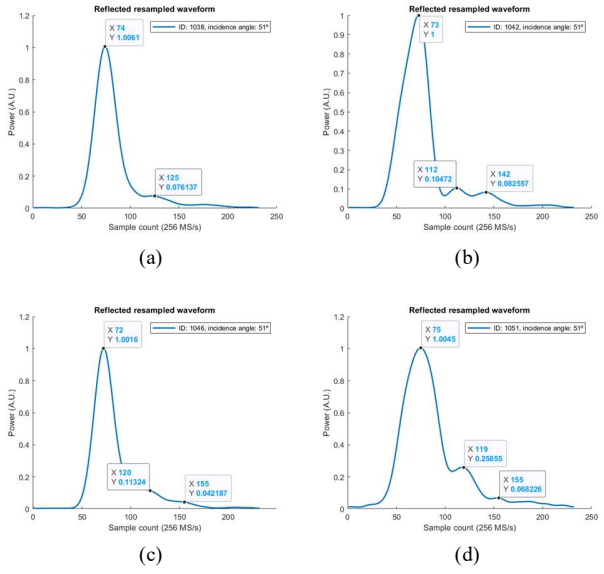

Fig. 6: GPS L5 reflected waveforms over the sea (beam 2) with a second peak present in the reflected waveform for case (a), two small secondary peaks for cases (b) and (d), and a blurry of the tail of the reflected waveform for case (c)

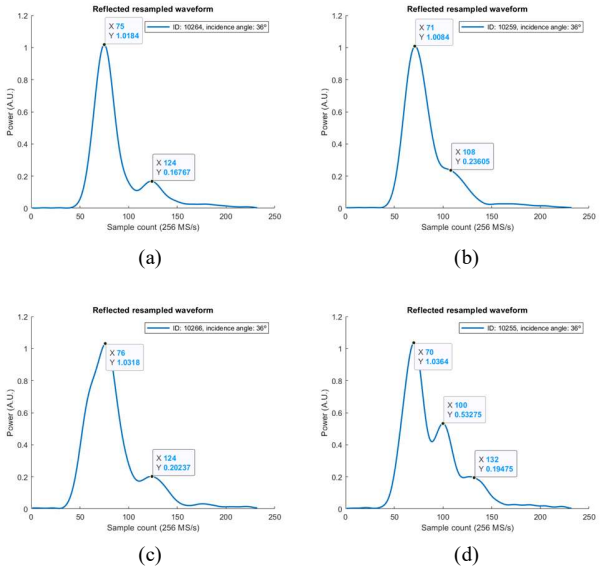

Fig. 7: Galileo E5a reflected waveforms over the sea with a second peak present in the reflected waveform for cases (a), (b), and (c), and two secondary peaks for case (d)

5. CONCLUSIONS

This work has presented the first experimental evidence of wind and swell waves signatures in GNSS-R waveforms as a second and third peaks in the reflected waveform. This new data from the GNSS-R data still requires further improvement and a more exhaustive analysis but, the results shown offer the promise for the use of L5/E5 GNSS-R signals to infer new geophysical parameters as the wave period or wavelength of the sea thanks to the shapes of the auto-correlation function.

6. ACKNOWLEDGEMENTS

This work was supported by the Spanish Ministry of Science, Innovation and Universities, “Sensing with Pioneering Opportunistic Techniques”, grant RTI2018-099008-B-C21, and the grant for recruitment of early-stage research staff FI-DGR 2015 and 2018 of the AGAUR - Generalitat de Catalunya (FEDER), Spain, and Unidad de Excelencia Mar´ıa de Maeztu MDM-2016-060.

7. REFERENCES

[1] R. Onrubia, D. Pascual, H. Park, A. Camps, C. Rüdiger, J. Walker, and A. Monerris, “Satellite Cross-Talk Impact Analysis in Airborne Interferometric Global Navigation Satellite System-Reflectometry with the Microwave Interferometric Reflectometer,” *Remote Sensing*, vol. 11, no. 9, pp. 1120, may 2019.

[2] R. Onrubia, D. Pascual, H. Park, and A. Camps, “Preliminary Altimetric and Scatterometric Results with the Microwave Interferometric Reflectometer (MIR) during its first airborne experiment,” in *ARSI-KEO 2019, ESA, Noordwijk, Netherlands*.

[3] Deutscher Wetterdienst (DWD), “Icon model description by dwd,” Available at: https://www.dwd.de. Last visited: 07 Jan. 2020.

[4] InMeteo, “Ventusky,” Available at: https://ventusky.com. Last visited: 07 Jan. 2020.

[5] U.S. Army Corps of Engineers, *Coastal Engineering Manual Part II: Coastal Hydrodynamics (EM 1110-2-1100)*, Books Express Publishing, 2012.

[6] Joan Francesc Munoz-Martin, Raul Onrubia, Daniel Pascual, Hyuk Park, Adriano Camps, Christoph Rüdiger, Jeffrey Walker, and Alessandra Monerris, “Experimental evidence of swell signatures in airborne l5/e5a gnss-reflectometry,” *Remote Sensing*, vol. 12, no. 11, 2020.